IEEE Access
Multidisciplinary ⋮ Rapid Review ⋮ Open Access Journal

Received 3 August 2023, accepted 18 September 2023, date of publication 22 September 2023, date of current version 4 October 2023.

Digital Object Identifier 10.1109/ACCESS.2023.3317980

RESEARCH ARTICLE

Operation of Grid-Connected PV System With ANN-Based MPPT and an Optimized LCL Filter Using GRG Algorithm for Enhanced Power Quality

NAGWA F. IBRAHIM[1], MOHAMED METWALLY MAHMOUD[2], ALI M. H. AL THAIBAN[3], ABDULWASA B. BARNAWI[4], Z. M. S. ELBARBARY[4], AHMED IBRAHIM OMAR[5], AND HANY ABDELFATTAH[1]

[1]Electrical Department, Faculty of Technology and Education, Suez University, Suez 43533, Egypt
[2]Electrical Engineering Department, Faculty of Energy Engineering, Aswan University, Aswan 81528, Egypt
[3]Ministry of Health, Riyadh 11176, Saudi Arabia
[4]Electrical Engineering Department, College of Engineering, King Khalid University, Abha 61421, Saudi Arabia
[5]Electrical Power and Machines Engineering Department, The Higher Institute of Engineering at El-Shorouk City, El-Shorouk Academy, Cairo 11837, Egypt

Corresponding authors: Mohamed Metwally Mahmoud (metwally_m@aswu.edu.eg) and Ahmed I. Omar (a.omar@sha.edu.eg)

This work was supported by the Deanship of Scientific Research, King Khalid University, under Grant RGP2/309/44.

ABSTRACT The expanding use of photovoltaics (PV) as a green energy resource has been rising in these years, mostly due to the possibility of being incorporated with traditional power systems, to meet the world's energy needs and reduce carbon emissions. However, providing green electricity from this renewable generator is frequently vulnerable to power quality (PQ) disruptions resulting from the PV's intermittent nature and other factors associated with the electric grid, power converters, and linked loads. These disruptions need to be reduced to keep the investigated system's PQ from deteriorating. The investigated system includes PV, DC-DC, and DC-AC converters, filter, power grid, and control schemes. If the DC-DC converter is not managed, a deviation from the maximum power point (MPP) extrapolated from the PV system will take place. In order to maximize the energy harvested from the PV system by managing the DC-DC converter, this research developed two MPP tracking (MPPT) algorithms: artificial neural networks (ANN) and cuckoo search (CS). Additionally, a design and implementation for a shunt active power filter (LCL) using genetic algorithm and GRG is provided to lower the injected total harmonic distortion (THD) and thereby enhance the PQ. To achieve the smallest size of the LCL components, the generalized reduced gradient (GRG) was the best compared to genetic algorithms GA. The results of the simulation showed that ANN performed better at tracking maximum power than CS. With the designed LCL, the THD is reduced by 99.78% compared to without a filter. To verify the simulation's findings, a practical configuration is implemented.

INDEX TERMS Artificial neural network (ANN), Cuckoo search (CS), LCL filter, MPPT, total harmonic distortion (THD).

I. INTRODUCTION

The utilization of renewable energy sources (RESs) especially solar (PV) has increased and evolved globally since they are a clean and secure alternative [1]. It is a cutting-edge replacement for fossil fuels, which will ultimately exhaust. First off, before they became more prevalent in domestic appliances, electrical grids, communications, and vehicles, PV panels were mostly used in big factories and missions in space [2], [3]. Reference [4] examined the development of PV technologies with regard to the cell materials used and the ambient conditions impacting the efficacy of PV cells. PV systems have the capability to operate in off-grid and on-grid modes. As a potential substitute for traditional non-RESs

The associate editor coordinating the review of this manuscript and approving it for publication was Norbert Herencsar.

and pollution-free, grid-connected PV (GCPV) technology has caught the interest of corporations and academia.

One of the most RESs of electricity for future energy generation has been thought to be PV systems. These systems use photon energy to create electrical energy. Since these sources produce low voltage output, high step-up dc/dc converters are utilized in a variety of applications, such as fuel cell technology, wind power, and solar systems, to convert low voltage into high voltage [5], [6]. PV must have become an attractive alternative as a result of both the increasing demand for electricity and the expensive and limited supply of traditional energy sources. Availability, zero emissions, and low operation and maintenance costs are all advantages. The utilization of PV energy systems, both in their independent and grid-tied forms, must be increased as a result [7], [8]. PV appears to be essentially unreliable due to location, timing, months, and atmosphere, however, it is also still quite costly to execute. PV panel efficacy appears to be much improved by running the system near to its maximum power point (MPP) in order to obtain the anticipated highest power output [9].

The GCPV's generated power is impacted by weather fluctuation; thus, it cannot operate at its maximum capacity. Scholars are looking into methods of maximum power point tracking (MPPT) to ensure that PV systems function at MPP under fluctuations in weather as a result of the subsequent fall in the efficacy of energy conversion [10], [11]. Different MPPT approaches are used together with power electronic equipment under uniform radiation; the most popular online strategies are perturbed and observe (P&O), hill climbing (HC), artificial neural network (ANN), fuzzy logic, and incremental conductance (IN) [12], [13], [14]. Additional indirect (offline) methods involving constant voltage, constant current, and curve fitting have been thoroughly explained in [15] and [16]. Hybrid algorithms have been used, as shown in the case of partial shading or non-uniform radiation [17], [18].

One of the primary issues with using PV power systems, particularly at the point of common coupling (PCC), is the power quality (PQ) [19]. The primary sources of PQ problems, specifically the creation of voltage and current harmonics, are variable solar irradiation, grid faults, and nonlinear loads with advanced power electronics equipment. Unwanted effects of harmonic distortion (HD) on the power grid include interruption of the grid's regular operation, overheating of linked devices, reduction in electrical meter accuracy, interfering with lines of communication, and a rise in the demanded current [20], [21]. Reference [22] studied the similarities and differences between Brazilian standards for GCPV inverters and comparable standards in Europe and the US. Reference [23] analyzed the voltage and current HDs at the PCC of a GCPV system applying the ICA method. A harmonic management technique was suggested to keep the total HD (THD) within the acceptable range after an assessment of the prevalence of the current THD in the GCPV structure [24].

The major power components of a typical GCPV system appear to be the inverter and the passive filter. Although MLIs are preferred in 3-phase systems, particularly for big power applications when the switching frequency is low, a current-controlled two-level inverter has traditionally been used as a power conditioner in modest energy household setups. When those systems are used, the grid is exposed to the undesirable harmonic currents produced by the inverter, which lowers the system's efficiency. As a consequence, a number of standards, including IEEE-519 and IEEE-1547, were developed to restrict the entry of undesired harmonics into the grid [20], [25]. A low-pass filter is required to put between the inverter and the grid for all power levels to meet the criteria of these standards [26]. Constructing the ideal passive filter for grid-based systems is not a simple task due to a number of factors, such as the possibility of resonance between the filter circuit and system impedance [27], [28]. It is a challenging problem that cannot be assured by standard design methods to find the optimal first-order L-filter implementation that meets the needed requirements while remaining as affordable as possible [29]. High-order topologies of passive filters will provide greater harmonic attenuation at lower total inductance rates as a result, which will decrease the filter's size and cost [30]. Changes in solar irradiance and switching devices with cutting-edge power electronic units are the main causes of power flaws, particularly the production of both voltage and current HDs [31].

HDs in electrical systems have been eliminated using a variety of methods, including passive and active filters. Reference [32] showed that an LCL filter with a shunt damping resistor reduced THD to 0.26%; as a result, it performed better than the L and LC structures in mitigating harmonics. In [33], a parallel RC circuit and a digital filter were used to show the hybrid damping approach. Reference [34] a shunt active filter and the d-q regulating method were used for a developed GCPV system to minimize the current THD from 27.3% to 3.9%. In [35], a hybrid damping strategy's properties using a combination of passive and active damping approaches, achieving the current THD value of 3.7%. Reference [36] investigated the d-q shunt active filter and INC approach for MPP monitoring used to keep current THD within acceptable ranges. For the DC bus voltage management, the suggested study used the ANN controller rather than the traditional PI controller. Simulated results from this approach demonstrate that the existing THD was decreased to 3.2%. For harmonic suppression, there are numerous alternative techniques besides filters that could be helpful. In [37], when the 127- multi-level inverter (MLI) was compared with MLIs of lower levels, the current THD was decreased to 2.33% by the 127-level MLI. The operation of the pulse width modulation (PWM) inverter and its resulting energy efficiency of a GCPV system was improved with the direct power control methodology. The findings demonstrated that this strategy had positive repercussions. The operation of the pulse width modulation (PWM) inverter and its resulting

energy efficiency of a GCPV system were improved with the suggestion of a direct power control methodology. The simulation demonstrated that this strategy had positive repercussions [38]. The harmonic limitations for system voltages between 120 and 69 kV were presented in [39].

The main focus of this study is on developing a GCPV system in accordance with the aforementioned needs and standards criteria using intelligent techniques. The investigated configuration is constructed using a two-level converter, a boost converter, an LCL filter, and a PV array. The architecture of the management system in the d-q reference frame is covered. The results of an inverter, LCL filter, and MPPT algorithm are discussed along with an experimental implementation. These results also show that the current control strategy responds by lowering the harmonic voltage and current by 12.73 to 0.03% and 13.92 to 0.028%, respectively. The following are the significant discoveries and accomplishments:

- The application of two MPPT methods, namely the ANN and the cuckoo search (CS) approach, for GCPV systems, is a significant contribution made by this study. The duty cycle (D) of the DC-DC converter can be adjusted to reflect changes in the MPP by using ANN or CS to update the control signal. In this work, the suggested ANN and the CS techniques, are contrasted. The ANN method surpassed the CS algorithm in terms of performance and speed of dynamic responsiveness for MPPT in a number of control indices, including overshoot, rising time, and transient response.
- To keep voltage and current THD at the higher switching frequency within prescribed limits, an effective LCL filter is constructed. The LCL filter is designed with genetic algorithm (GA) and generalized reduced gradient (GRG) algorithms and the results prove the GRG superiority. The PCC shall give an appropriate level of PQ problems utilizing these complicated characteristics in accordance with the updated criteria. All PQ issues have been altered and deteriorated to the standard stated level as a result of the simulation findings by putting into place efficient controls and compliance mechanisms.

The paper is prepared as follows: section II, PV modeling is addressed; section III, the investigated MPPT techniques (ANN, and CS) are presented; section IV the GCPV is analyzed and the facing issues is presented; section V discusses the proposed filter design with GA, GRG, and conventional method; section VI the simulation, expermintal, and discussion of proposals are made; and as the last part, the conclusions are presented.

II. PV ARRAY MODELLING

The model based on one diode and the equivalent circuit is represented in Fig 1.

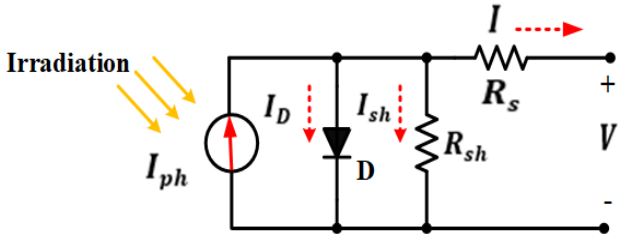

FIGURE 1. One diode equivalent circuit.

TABLE 1. Parameters of the used PV panel.

Parameters	Value
P_{PV}	100 kW
Open circuit voltage of one PV module (Voc)	64.2 V
Grid angular frequency (ω)	314 rad/s
Inverter carrier frequency ($\mathbf{F_C}$)	10 kHz
Sample time	1 µs
The inductance of the boost	5 µH
Dc-Link capacitance	2 × 12 mF
The reference voltage of the Dc-Link	500 V
The measured voltage of the Dc-Link	500 V

Current characteristics are given by the following equation [27]:

$$I_{pv} = I_{ph} - I_0 \left[e^{q\frac{(V_{pv}+I_{pv}.R_s)}{AkT_j}} - 1 \right] - \frac{V_{pv}}{R_{sh}} \quad (1)$$

where, I_{ph} is the photocurrent, I_o is the saturation current of the diode, I_{pv} is the PV output current, V_{pv} is the PV output voltage, T denotes junction temperature, A ideality factor, k=1.38e-23 Boltzmann's constant, q is chargeonanelectron=1.60e-19, and R_s, R_{sh} are serial and shunt resistances, respectively. The used photovoltaic panels have the following characteristics in Table 1. The obtained electrical characteristics are obtained by taking into account the effects of solar temperature variations, as depicted in Figs 2(a) and (b).

III. MPPT APPROACHES

Two tracking approaches are described in this subsection, they may be used to guide a PV system toward the best functioning point in the face of shifting environmental circumstances [40], [41].

A. ANN MECHANISM

Among the most effective artificial intelligence (AI) methodologies to model the behavior of ANNs in persons would be the artificial intelligence system. It serves as a paradigm for interpreting data [42]. A huge number of basic parts known as

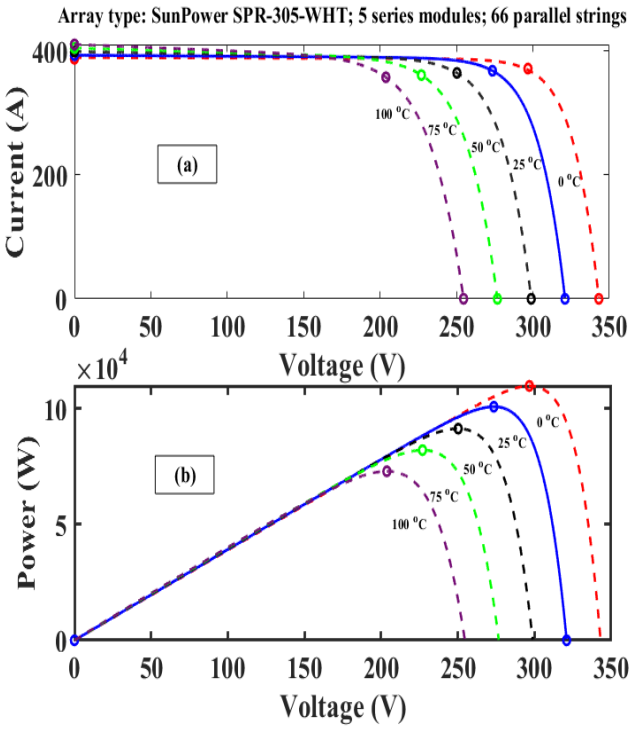

FIGURE 2. Characteristics of ($I_{PV} - V_{PV}$) and ($P_{PV} - V_{PV}$) under solar temperature variations.

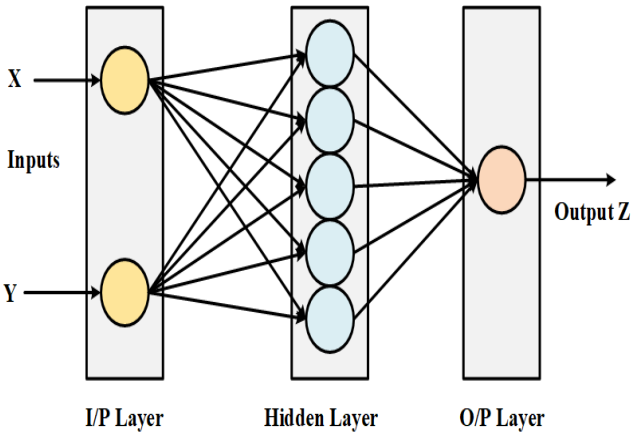

FIGURE 3. ANN Organization.

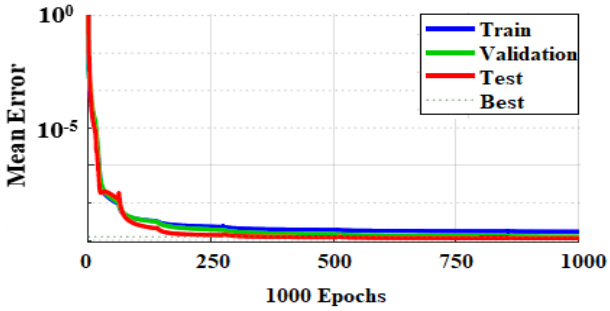

FIGURE 4. Following instructions, the mean error.

neurons help compensate ANNs, which also operate together concurrently to solve these issues.

This method determines the outputs as well as the goal repeatedly till the channel's output is identical towards the objective. Furthermore, retraining necessitates a substantial number of input/target combinations. Hidden, input, and output layers make up the three layers that make up an ANN, as shown in Fig. 3. The input layer takes received inputs as well as distributes these toward the hidden layer's synapses. The output layer creates a correct outcome of the ANN. Through input to output, a hidden layer does the intermediary computations. Following conducting various experiments, its architecture becomes finally decided upon [42].

Temperature (X) with irradiance (Y) have been chosen because quell inputs with both the help of 5 neurons located in the hidden layer as well as the output seems to be the duty ratio (Z) [39]. When developing the network, the input data set points have been gathered. At a steady 25°C, X ranges from 250 to 1000W/m^2 in increments of 250W/m^2. Y additionally ranges from 25 to 45 degrees Celsius at a steady 1000 watts per square meter.

But using the Logistic regression training algorithm method, Fig 4 depicts the mean error (ME) graph in off-retraining. There have been three data segments: 70 percent of the total for instruction, 15 percent respectively for confirmation, plus 15 percent of the total number for assessment. The performance will improve with decreasing ME [43], [44].

Especially in comparison to a fractional- order PID (FOPID) controller, this technique provides a rapid reaction as well as less fluctuation. ANN seems to be self-learning and therefore does not require retraining. The primary shortcoming of the ANN includes black box operating & sluggish retraining [45], [46].

B. CS MECHANISM

Another of the finest optimization meta-heuristic methodologies called CS, which also has gained popularity across automated systems [47]. Instance MPP, technology operates PV systems promptly and effectively [48].

The above methodology was influenced mostly by belligerent spawning as well as the bloodsucking attitude of cuckoo birds, who deposit their clutches in cooperative colonies or sometimes steal other birds' clutches to enhance the likelihood that their individual eggs would hatch [47].

A CS technique has always been based on three guidelines: either every cuckoo might only lay one egg contains in a random selection nest, the greatest nest in the initial iteration with slightly elevated eggs (i.e., with the cheapest options of the decision variables) will pass toward the following generation, and the host bird can find the cuckoo's egg inside another nest with something like a statistical likelihood Pa therefore ($0 < Pa < 1$).

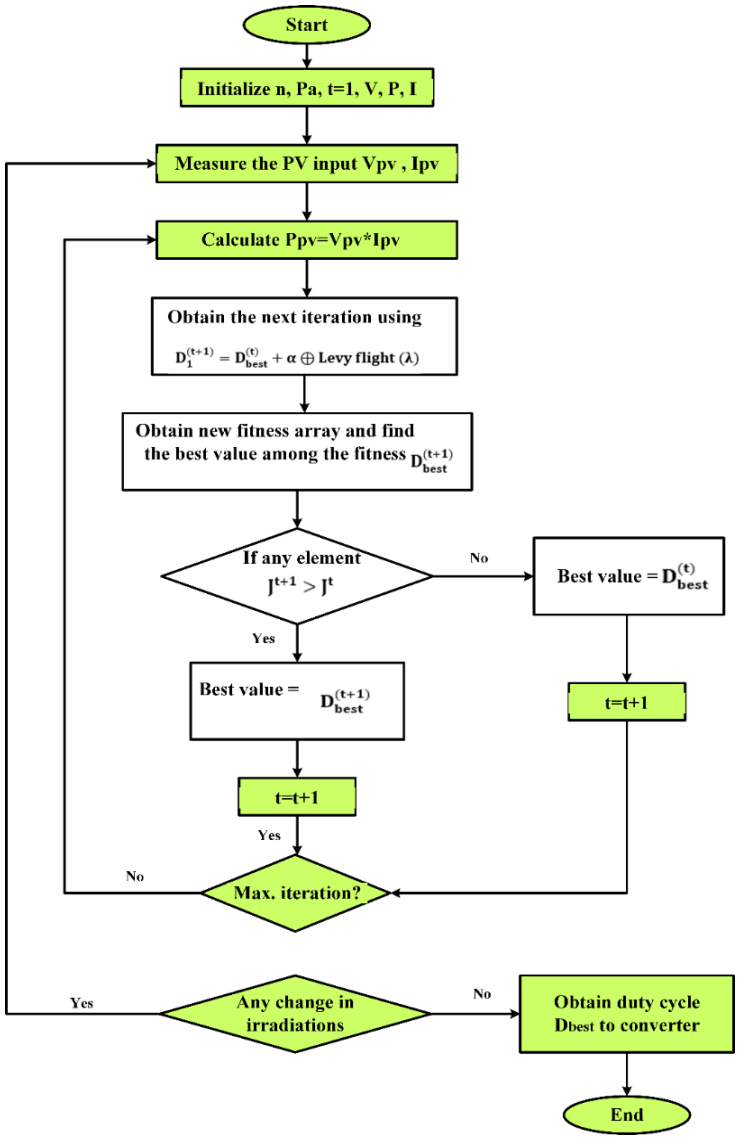

FIGURE 5. Flowchart for the CS algorithm.

A presenter bird's strongest clutch is randomly sought throughout the selection process. It could possibly be designed after the Based optimization flight mathematical theorem. Figure 5 is an implementation of the CS chart. PV power (PPV) and current (IPV) have been monitored and serve as parameters within that approach. An outcome seems to be the control signal (D), which may be adjusted using Lévy flight as follows [49]:

$$D_i^{(t+1)} = D_{best}^{(t)} + \alpha \oplus Levy\,flight(\lambda) \tag{2}$$

Because once I is indeed the sampling quantity, t seems to be the number of iterations, α is really the staging process ($\alpha > 0$ also presumed that $\alpha = 1$), as well as the combination indicates entrance-wise matrix multiplication. $D_{best}(t)$ represents samples/eggs or the best duty cycle among the fitness. Anyone would decide the amount of α as follows:

$$\alpha = \alpha_0(X_j^{(t)} - Xi^{(t)}) \tag{3}$$

Levy dispersion using the power function is employed to estimate the step length, from which:

$$Levy\,(\lambda) \approx u = L^{-\lambda} where(1 < \lambda < 3) \tag{4}$$

IV. A GRID INTEGRATED SYSTEM UNDER INVESTIGATION

Figure 6 displays the setup of the component for the system under test. Two mechanisms are advised for PV systems that are connected to the electrical grid. The PV's power is controlled in the first stage by a DC-DC converter. This allows for maximum power requirement in the normal case or MPPT mode. The second step is composed of a two-level

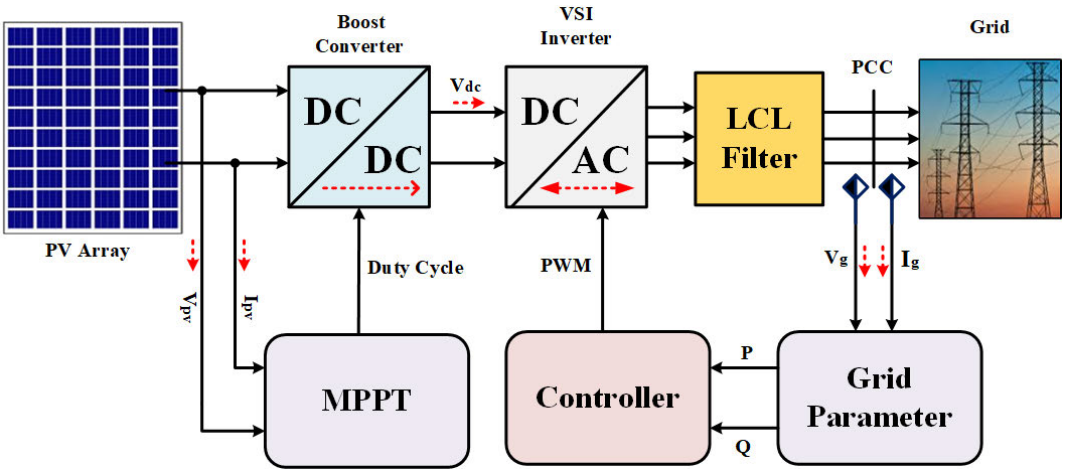

FIGURE 6. Architecture of PV installations that are connected to the grid.

three-phase Voltage Source Converter (VSC) and a DC/AC inverter. The DC link of the VSC has been coupled to the boost converter's output. The three-phase VSC consists of three Insulated Gate Bipolar Transistor (IGBT) legs. The LCL filter's other end is connected to the common connection point, and the VSC's output terminals are coupled. Fig. 6 displays the management diagram for the PV-connected system that was employed in this study. The boost converter management, as well as the grid-tied inverter control, are the two key components of the state's control. The configuration MPPT is suggested for boost control. The recommended system's first stage aims to increase the voltage output to the desired level and configure the PV's controller parameters to its maximum power operating point. Current, power, MPPT, and voltage collapse sensing are all parts of the control module. The system filter's three-phase perspective is seen in Fig. 7.

A. PV-HD REQUIREMETS

The distortion for voltage and current waves that causes particles to diverge beyond their normal characteristics or shapes is referred to only as frequency deviation. It is always often seen as a serious PQ problem. Due to the installation of inverters, converters, as well as other power electronic devices, oscillations would occur in a PV system. Different power-electronic elements contained in the PVs contribute generate distortions throughout this situation [50]. Excessive both voltage and current disturbances' magnitude also contribute to additional network failures as well as the breakdown of grid-side protective devices. To ensure that harmonic content somewhere at PCC is maintained to a minimal, stringent rules seem to be in place. According to [47], HD may indeed be defined and measured using the THD of either voltage or current. With the exceptions of ERECG83 and VDE-AR-N4105, as these are extremely strict and demand a THD for PV assimilation compared with fewer than 3% [51], various HD standards are implemented all across the development of PV system process automation throughout into grid. Despite this, those that are equivalent. The distortion restrictions regarding current and voltage that have to be acquired at PCC are summarized in Tables 2 and 3, correspondingly.

TABLE 2. Current HD limits of the PV systems.

Standards	Type	(h)	Distortion limit	THD (%)
IEEE i547as477 7.2(Australia, China, Malaysia)	Odd	33<h	<0.3%	<5%
		23≤h≤33	<0.6%	
		17≤h≤21	<1.5%	
		11≤h≤15	<2%	
		3≤h≤9	<4%	
	Even	10≤h≤32	<0.5%	
		2≤h≤8	<1%	
UK (EREC G83 stds.)	Odd	h=3,5, & 7	< (2.3, 1.14, & 0.77) %	<3%
		h=9,11, & 13	< (0.4, 0.33, & 0.21) %	
		11≤h≤15	<0.15%	
	Even	h=2,4, and 6	< (1.08, 0.43, & 0.3) %	
		8≤h≤40	<0.15%	
IEE 61000-3-2	Odd	h=3,5, & 7	< (3.45, 1.71, & 1.15) %	<5%
		h=9,11, & 13	< (0.6, 0.5 & 0.3) %	
		15≤h≤39	<0.225%	
	Even	h=2,4, & 6	< (1.6, 0.65, & 0.45) %	
		8≤h≤40	<0.345%	

TABLE 3. Voltage HD limits of the PV systems.

Standards	Voltage bus	Max. individual harmonics	THD (%)
IEEE 519	(V≤1) kV	5%	8%
	(1≤V≤69) kV	3%	5%
	(69≤V≤161) kV	1.5%	2.5%
	(V>161) kV	1%	1.5%
IEC 61000-3-2	(2.3≤V≤69) kV	3%	5%
	(69≤V≤161) kV	1.5%	2.5%
	(V>161) kV	1%	1.5%

The control system provides responsible for managing and adhering to current rules pertaining to voltage fluctuation, voltage sag, distortions, voltage mismatch, frequencies, and power factor in order to keep grid stability [50]. In conclusion, in order to confirm authentication and accordance only with

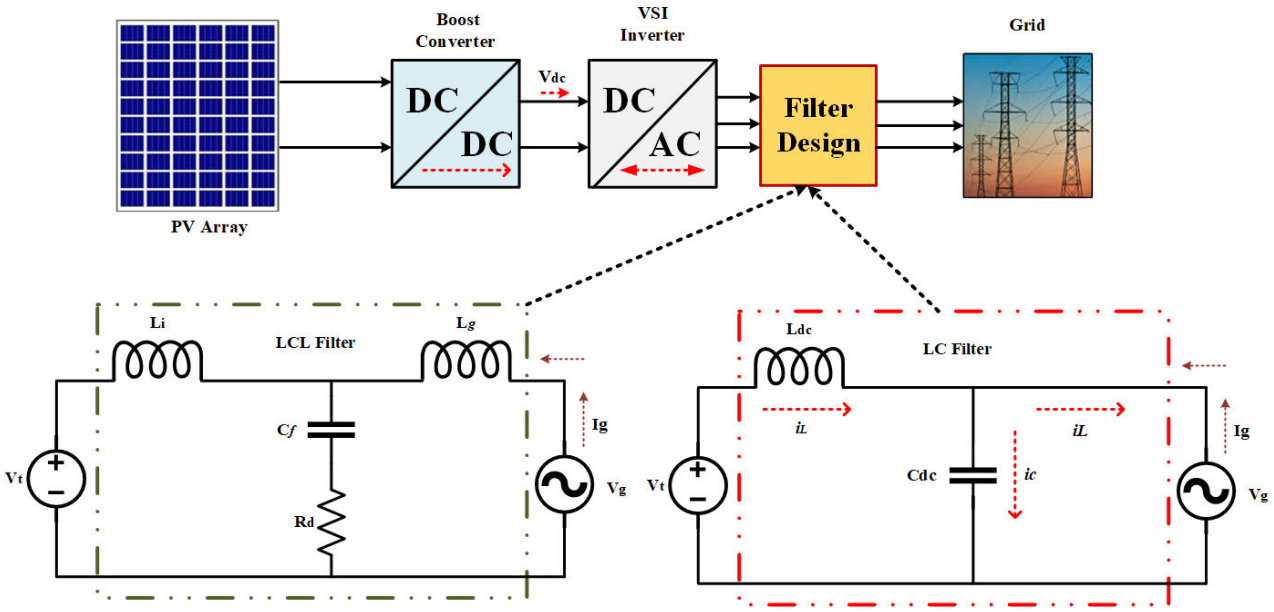

FIGURE 7. The integrated PV system's control diagram for filter design.

previously discontinued incorporation requirements, the PVs need to employ the PQ requirements set certification confirmation. Throughout this regard, this division evaluates and controls the power quality of massive PV systems connected to the distribution network online with applicable PQ regulation changes.

B. REDUCTION OF HARMONICS ACCORDING TO THE REQUIREMENTS OF THE STANDARDS

The control and structuring methodologies could have a positive or negative influence mostly on oscillations output. CS installations must be clearly cultivated in accordance with the most contemporary requirements as a consequence. The huge control system is connected to such an HV side (11 kV) throughout this experiment, as stated in Section III. Per the harmonic guidelines (Table 2 and 3), the total THD there at PCC must be lower than 5%, whether it be for current harmonic current (I-THD) or voltage harmonic distortions (V-THD), with the exception of UK requirements, whose call for the I-THD to be lower than 3%.c In this study, the THD of something like the PVs current waveform (voltages and currents) around PCC is evaluated and calculated using the fast Fourier transform (FFT) simulation software tool to record particular harmonics. Mostly in construction process to lower oscillations, the following methodology and tactics have been taken into account: In order to reduce output, I-THD and V-THD, the self-commutated PV inverter, a standard conversion of the GCPV with a DC-DC converter, current-controlled PV inverters, voltage-controlled PV inverters, current-controlled PV inverters, current-controlled PV inverters, PWM switching, and harmonics reduction are all used. But at the other hand, the I-THD and V-THD oscillated at a rate of around 22.22 and 6.72 percent over the standards' tolerances, respectively. The PWM carrier frequency is increased while an appropriate LCL filter is built to reduce the harmonic level.

V. DESIGN CRITERIA FOR PASSIVE GRID FILTERS

A. CONVENTIONAL DESIGN

To be able to meet the requirements of the standards, the major objective of grid filter design (GFD) methods is to absorb current harmonics to specific acceptable values defined by the relevant specifications. Traditional GFD standards are meant to include some factors when determining the proper rating for the passive elements as presented in [46], [47], [52], and [53].

B. GA METHOD

GAs are evolutionary methods that can be utilized to find the optimal solution for the creation function of an enhancement task. Holland first proposed GAs, computer programmers that mimic the course of natural evolution, in 1970. Every iteration of GAs alters a population of people, with each additional person serving as a stand-in for a potential solution to the issue. Those in the population who are physically fit live to reproduce, recombining their genetic material to produce new humans as offspring. Modeling the genetic material involves using some type of data structure, most typically a small number of features. Like in nature, the decision provides the necessary drive.

A fitness estimate is given to each remedy, indicating how efficient it is in comparison to other options in individuals [49]. The recombination procedure is mimicked by a crossover mechanism that exchanges sections of data strings

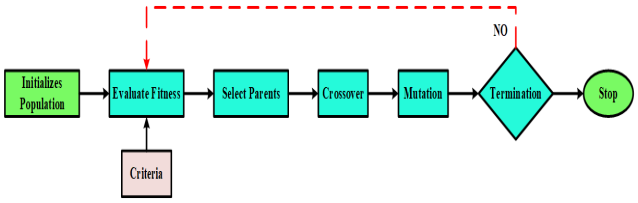

FIGURE 8. Basic GA cycle.

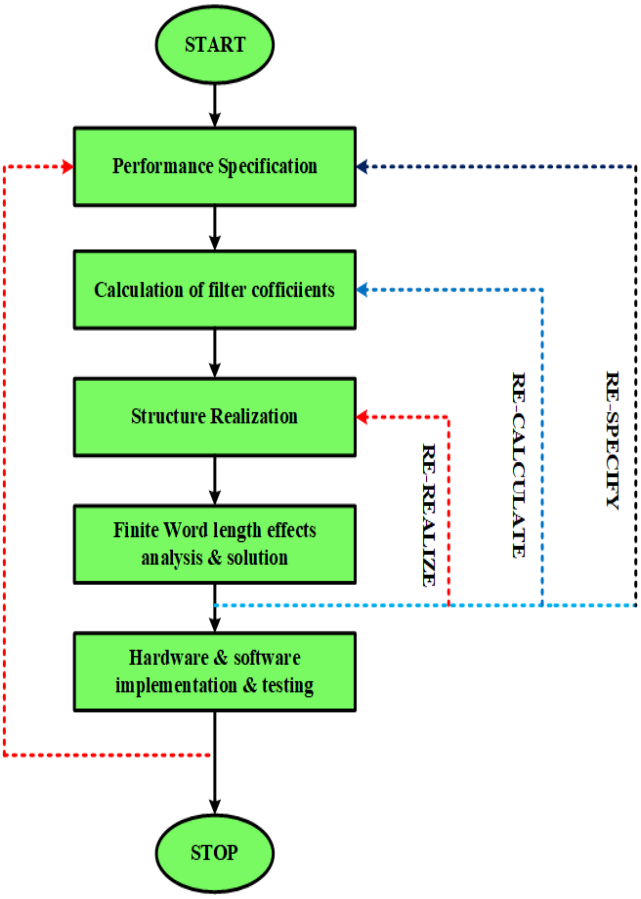

FIGURE 9. Flow chart of digital filter (DF) design.

between the chromosomes. A mutation that causes the strings to change randomly also adds new genetic material [54]. Only when a specific preset probability is satisfied to do these genetic processes happen frequently. As depicted in Fig. 8, the selection, crossover, and mutation processes make up the basic GA cycle or generation [55], [43]. This cycle is continued until a set of predefined conditions are satisfied. Owing to developments in electronic circuit technological advances, the model of developing systems becomes more and more feasible, and GAs have been used for a variety of real-world difficulties, such as GFD as depicted in Fig 9.

Since nonlinear and multimodal error surfaces are frequently present in digital infinite-impulse response (IIR) filters, it is vital to employ global optimization techniques to avoid local minima. In order to ensure the filter's stability while permitting the magnitude response to approximate a targeted characteristic, the values of ai and bi must be selected carefully. So far, scientific research has paid very little focus on the application of GAs in analog filters (AFs) [56]. A range of practical challenges must be taken into account when designing an AF [14], [18]. One of them is choosing the component values. A conventional type of GA is used in the design of the IIR- DF. The GA-based IIR-DF is made utilizing selection, crossover, and mutation. The range [0.19, 0.79] of the selected random number has been shown to be adequate. Fitness is evaluated in the standardized frequency range [0,1] over a regular grid of frequency points. The choice is the procedure of choosing components from the current generation to replace them in the following. The filter's structure uses the selection function, which assigns a portion of the wheel to each person based on their level of fitness. The procedure of having a child from two parents involves replacing a piece from one parent with the corresponding part from the second parent, and vice versa. Upon getting married, double point crossover produces filters between pairs of individuals and then yields the present generation. A mutation is an alteration introduced to some of the children generated by the crossover procedure by arbitrarily altering the value of one of the bits. The advantage of this method is that it can restore lost genetic values when the population converges too quickly. The filter parameters were stored as a 16-bit binary string with a population size of 50 with starting crossover probabilities and mutation probabilities of 0.7 and 0.03, correspondingly. The filter values produced by the GA filter follow the templates for phase as well as magnitude. The group's fitness value for the option I is determined by employing the given fitness equation [57]:

$$fit\ (i) = \frac{1}{k + J(w)i} \tag{5}$$

where J(w), and K are the cost function value, and the number of poles outside the unit circle, respectively.

C. GRG TECHNIQUE

GRG is a useful technique for getting the best result. The goal of GRG is to get the lowest values of L_1, L_2, and C under the assumption that THD is permitted. One way to describe the goal function for GRG optimization is as follows [18], [58]:

$$minf\ (x) = \left(1 + \frac{1}{r}\right) L_2(x = [L_2, r, C]) \tag{6}$$

The IEEE Standard 1547 clarify the permitted range of THD. The specification specifies that THD cannot exceed 5%. The restrictive value of THD might be set at 4.5% to depart a specific margin. The restriction is stated as:

$$THD\ (x) = 4.5\% \tag{7}$$

The f(x)'s reduced gradient is written as

$$gra\ (x) = \nabla f\ (x) \tag{8}$$

Considering that x_1 is the first iteration, the value becomes x_k after k repetitions. The possible drop route at the site is represented as follows:

$$(p_k)f = \begin{Bmatrix} -(xk)_j gra_j(xk) & gra_j(xk) > 0 \\ -gra_j(xk) & gra_j(xk) \le 0 \end{Bmatrix} \quad (9)$$

Describe a higher bound of the coefficient which is written as:

$$\alpha_{max} = min\left\{-\frac{(xk)_j}{(pk)_j}\right\} \quad (10)$$

The coefficient α that satisfies min $f(x_k+p_k)$ can therefore be obtained in the range [0, α max]. Fig. 10 depicts the GRG's flowchart. The termination condition of iteration is that THD (x_k) equals 4.5%. Here, xk is the outcome of the optimization. Based on this, the permitted range for L_1, L_2, r, and C are $0.0358 \le L_2 \le 0.0133$ mH, $120 \le r \le 152.12$, 1.87e-08 $\le C \le$ 3.97e-08 μF, $0.0158 \le L_1 \le 0.0221$ mH.

The optimized result is [0.0133 mH, 0.0221 mH, 152 and 3.97 μF] for the original value of x1 of [0.0112 mH, 0.0221 mH, 152 and 3.97e-08 F]. The capacitor has a sequence of fixed values in its actual state. 4 μF is the temperature that is most similar to 3.97 μF. Consequently, 4 F is chosen as the value of C. The parameters of the LCL filter are [0.01 mH, 0.03 mH, 152, and 4 μF] when the fixed value of C participates in the GRG.

D. LC-FILTER DESIGN

The limitation of the LC filter is that the shunt element is ineffective when connected to a stiff grid network, where the grid impedance is insignificant at the switching frequency. The output current ripple is the same as the inductor current ripple with an L-filter, where the attenuation depends solely on the filter inductance. The LC filter in Fig. 7 is a second-order filter giving –40 dB/decade attenuation. Since the previous L-filter achieves low attenuation of the inverter switching components, a shunt element is needed to further attenuate the switching frequency components. This shunt component must be selected to produce low reactance at the switching frequency. But within the control frequency range, this element must present a high magnitude impedance. A capacitor is used as the shunt element. The resonant frequency is calculated from (11).

$$f_0 = \frac{1}{2\pi}\frac{1}{\sqrt{LC}} \quad (11)$$

The LC type has been investigated in UPS systems with a resistive load [25]. This LC filter is suited to configurations where the load impedance across C is relatively high at and above the switching frequency. The cost and the reactive power consumption of the LC sorts are more than the L filter because of the addition of the shunt element.

E. LCL-FILTER DESIGN

Switching loss frequencies for both converters could be employed because the LCL filter attenuates at frequencies exceeding the maximum resonance frequency by 60 dB/decade. Furthermore, the design offers less ripple current from across network inductance as well as greater dispersion between both the bandpass and network impedance. LCL filter is nevertheless appropriate for our purpose. Although with minimal inductance settings, the LCL filter demonstrates better current fluctuation dampening. The mechanism may indeed experience resonant frequencies and unsustainable behaviors as nothing more than a result. As a result, the filtering needs to still be exactly created using the characteristics of the particular converter. There are several papers somewhat on the construction of LCL filters in scientific articles. The filter's break frequencies are a crucial element. Since this filtering requires to achieve sufficient dampening inside this area of something like the converter's cutoff frequency, the latter's cut-off frequency should be at least half of that frequency. Additionally, there needs to be enough space between the cut-off frequency and the grid frequencies. This same LCL filter's cut-off frequency could well be determined using:

$$F_{res} = \frac{1}{2\pi} * \sqrt{\frac{L_i + L_g}{L_i * L_g * C_f}} \quad (12)$$

Additionally susceptible to disturbances, the LCL filter might amplify harmonics close to its cut-off frequency. As a result, attenuation is introduced to the filter. Another easiest method is to include a dampening resistance. That resistance could be placed in parallel to the inductor on the side of the converter perhaps in parallel or in series to the filter capacitor in one of four possible locations. The decision was made decided to use a series resistor in conjunction well with a filter capacitor. The absorption resistor's value may very well be computed using,

$$R_{sd} = \frac{1}{3\omega_{res} * C_f} \quad (13)$$

Essentially nothing remains of the maximum somewhere at frequency response. This method is a straightforward as well as dependable method, but somehow it significantly reduces the filter's effectiveness and raises the system's thermal losses. Active attenuation may be employed to remedy this issue. The potential throughout the capacitor is decreased mostly by resistance by something like a value proportionate to the current flowing through everything. Moreover, this seems to be possible in the controlled system. The word monitors and distinguishes the current by C_f.

Rather than employing an actual resistor, this same estimated value is deducted from either the required current. With no losses, the filter is actively damped in this manner by a synthetic resistor. The above theory's weaknesses comprise the need for an extra current sensor or the possibility of noise issues due to the differentiator's amplification of high-frequency impulses [28]. The LCL filter featuring lowering resistance shown in Fig. 11 has been studied in terms of investigation and evaluation methods.

$$L_i = \frac{V_{dc}}{16F_s * \Delta I_{L-max}} \quad (14)$$

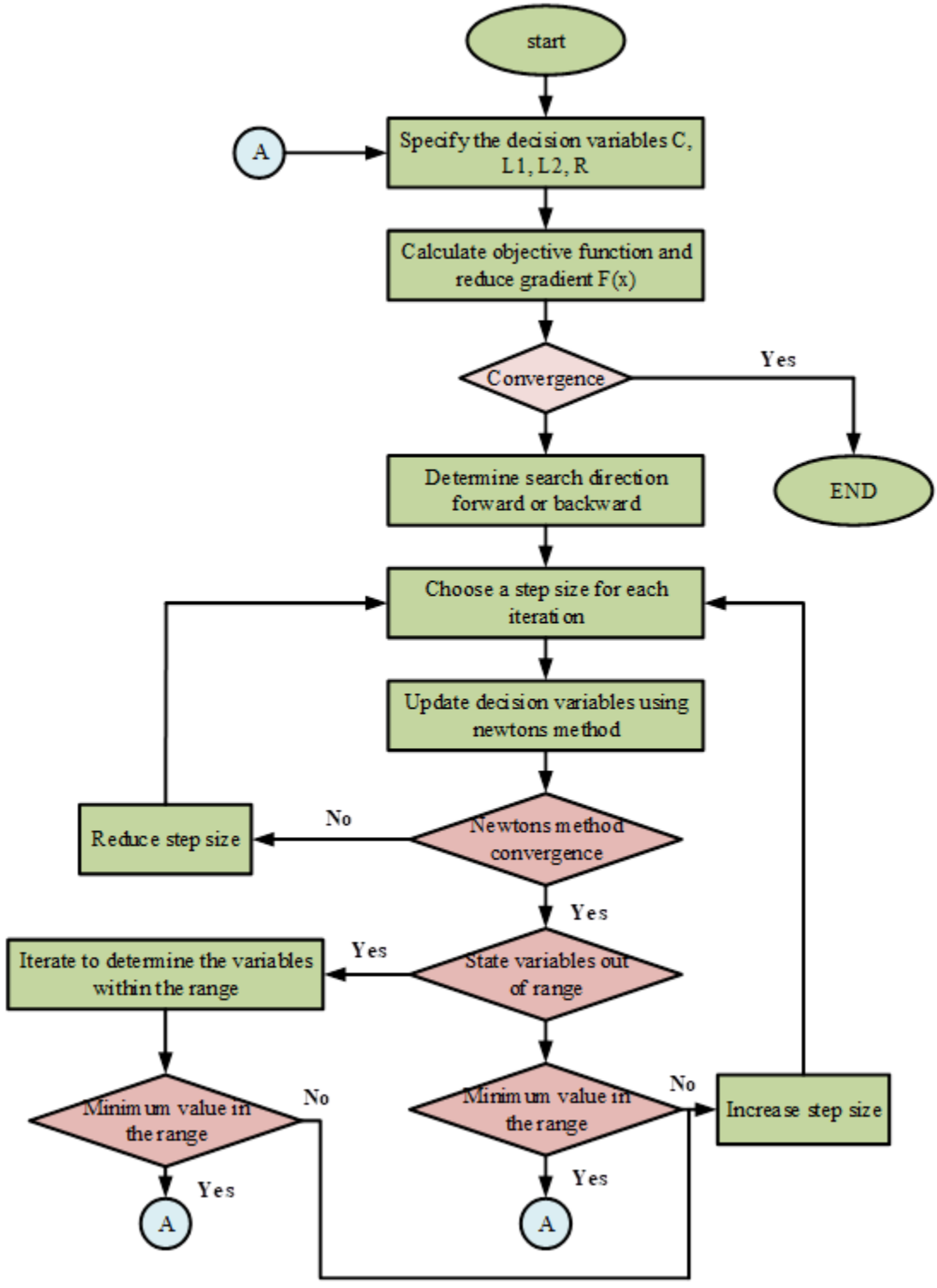

FIGURE 10. Flow chart of GRG technique.

where ΔI_{L-max} is the 10% current ripple specified by:

$$\Delta I_{\mathrm{L-max}} = 0.01\frac{\mathrm{P_n} * \sqrt{2}}{\mathrm{U_n}} \tag{15}$$

$$\mathrm{C_f} = 0.05{*}\mathrm{C_b} \tag{16}$$

$$\mathrm{Z_b} = \mathrm{U_n^2}/\mathrm{S_n} \tag{17}$$

$$\mathrm{C_b} = {}^{1}\!/_{\omega_n * \mathrm{Z_b}} \tag{18}$$

$$\mathrm{L_g} = \mathrm{r}{*}\mathrm{L_i} \tag{19}$$

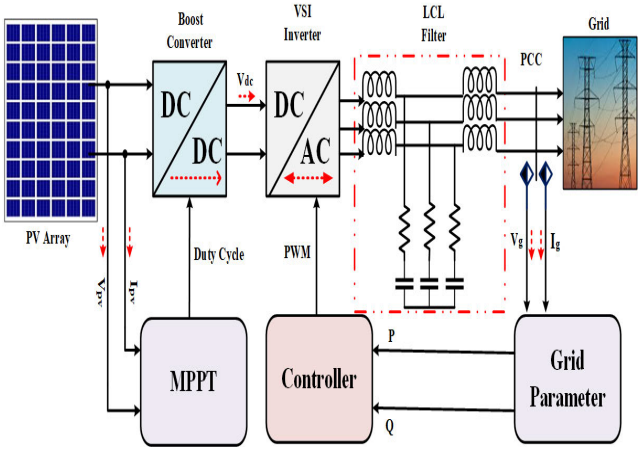

FIGURE 11. Schematic diagram of LCL filter components.

TABLE 4. Performance and duty ratio evaluation comparing suggested approaches.

X(W/m^2)	500	740	922	1000
Y(^{0}C)	25	25	25	25
CS	0.474	0.476	0.479	0.481
ANN	0.493	0.4994	0.4997	0.5

VI. SIMULATION RESULTS AND ANALYSIS

The complete circuital model of the GCPV model is shown in Fig. 11. Firstly, a solar panel is fed to the DC-DC converter which is controlled by the MPPT techniques. Then the DC input is converted into three-phase AC using VSC so that it can be implemented with the grid. The output at the connection junction of the grid and inverter is shown in Fig. 11. In this case, the irradiance is increased from 500 to 1000 W/m^2 between 1 and 2 sec., and the temperature is kept constant at 25^{o}C. With this increase in the irradiance between 1 and 2 sec., the PV power and current are slightly affected by the variation in the irradiance as depicted in Figs. 11 and 12, respectively. The best profile with fewer oscillations is obtained when applying the proposed MPPT algorithm, ANN. PV voltage is slightly increased as shown in Fig. 13. The oscillations in this voltage profile are high when using CS, while using ANN, the oscillations are reduced with the superiority of ANN over CS. Fig.14 shows the duty cycle (D). Some control measures for the PV voltage, current, power, and D when using the two MPPT algorithms for test case 2 are summarized in Tables 4, 5, and 6. From this comparison, the proposed ANN could reach the highest MPP with the best profile for the PV power among the two algorithms. The CS algorithm could improve the profile of PV current, and voltage.

The model of the proposed control scenario is developed on MATLAB/Simulink platform. The proposed system is implemented on several conditions, such as steady state, grid voltage balanced, variable solar irradiation level, and distorted grid voltage condition. Fig. 15 shows that the system is

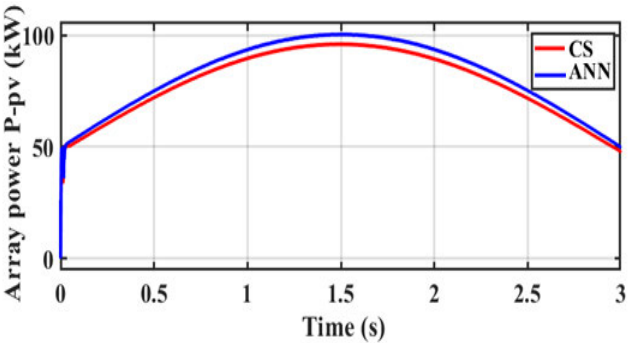

FIGURE 12. Array power (kW) at different techniques.

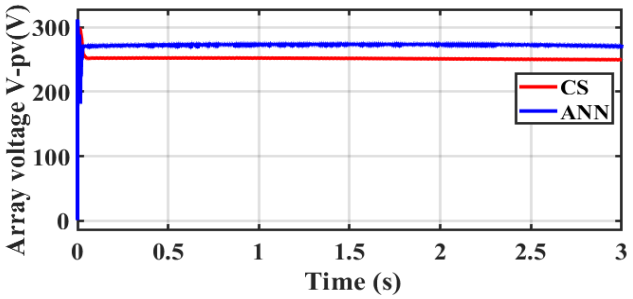

FIGURE 13. Array voltage (V) at different techniques.

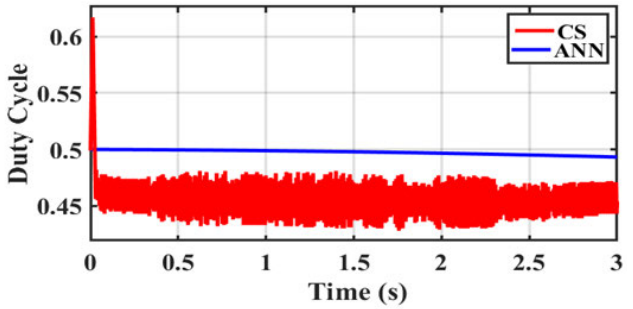

FIGURE 14. D with the investigated techniques.

TABLE 5. Assessment of the effectiveness of several suggested solutions in perspective of dynamic response and variation.

MPPT / Input	X(W/m^2)	500	740	922	1000
	Y(^{0}C)	25	25	25	25
CS	Tracking time oscillation (s)	0.023 medium	0.013 medium	0.009 medium	0.007 medium
ANN	Tracking time oscillation (s)	0.014 none	0.002 none	0.004 none	0.005 none

TABLE 6. Comparison of the suggested MPPT methods' total expenses and computation times.

MPPT Methods	Hardware Implementation		Cost	Sensed parameters	Software
	Type	Complexity			
CS	Digital	Complex	Medium	V & I	High
ANN	Digital	Complex	High	X & Y	Medium

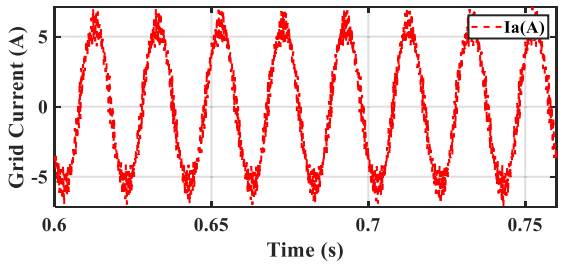

FIGURE 15. Output current signal without a filter.

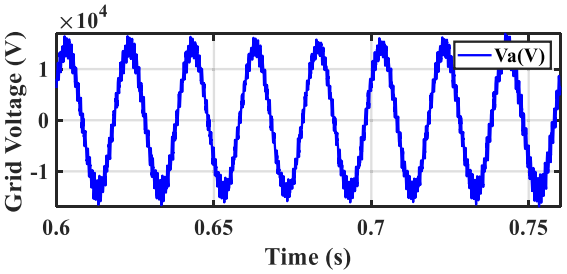

FIGURE 16. Output voltage signal without filter.

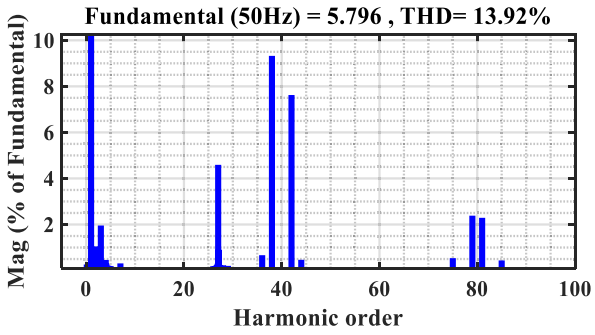

FIGURE 17. Harmonic spectra for output current signal without a filter.

running under variable solar irradiation level conditions. During this period the system is affected by harmonic distortion in voltage and current of the grid, to protect the grid from these harmonics a comparative LC and APF-based LCL filter is proposed. The outputs of the system without a filter are shown in Figs. 15 and 16. The THD of each voltage and current without a filter is shown in Figs. 17 and 18, respectively.

Figures 19 and 20 show the outputs of the system with an LC filter. The THD of each voltage and current with an LC filter is shown in Fig. 21 and Fig. 22, respectively.

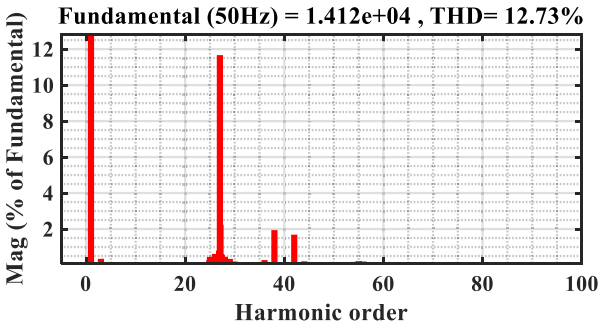

FIGURE 18. Harmonic spectra for output voltage signal without a filter.

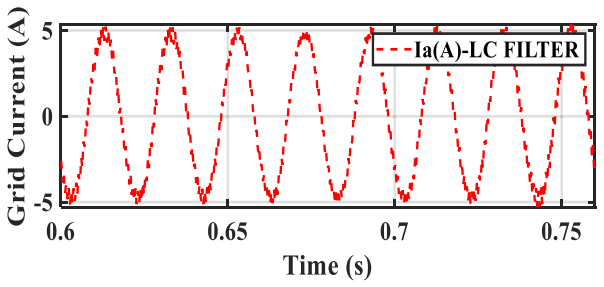

FIGURE 19. Output current signal with LC-filter design.

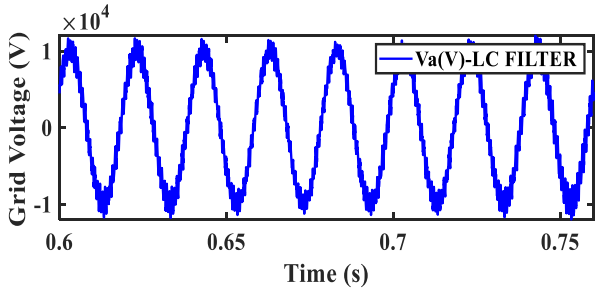

FIGURE 20. Output voltage signal with LC-filter design.

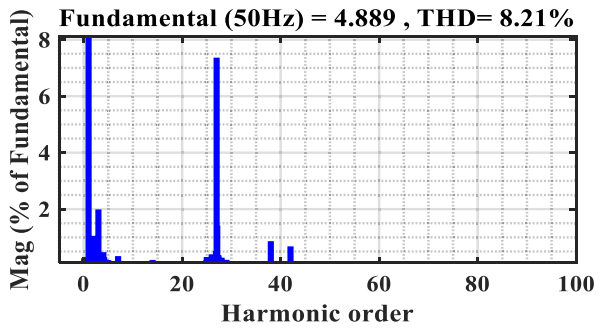

FIGURE 21. Harmonic spectra for output current signal with LC filter design.

From Figs. 21 and 22, we find that when using the LC filter, the THD of current decreased from 13.92 to 8.21 and that according to the current HD limits of the PV systems standard is rejected. We also find that the THD of voltage decreased using the LC filter in the waveform from 12.73 to 11.3, and

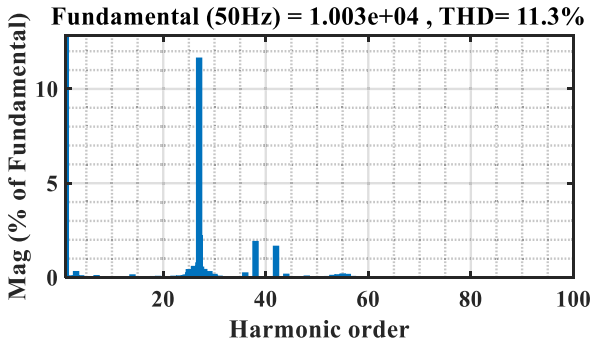

FIGURE 22. Harmonic spectra for output voltage signal with LC filter design.

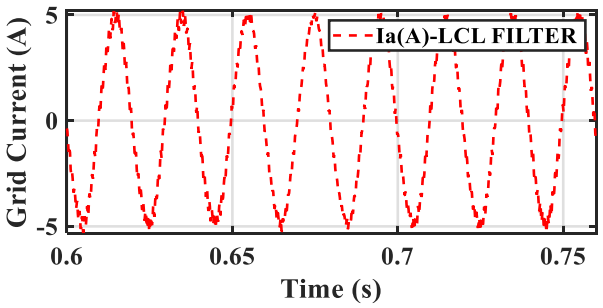

FIGURE 23. Output voltage signal with LCL-filter design.

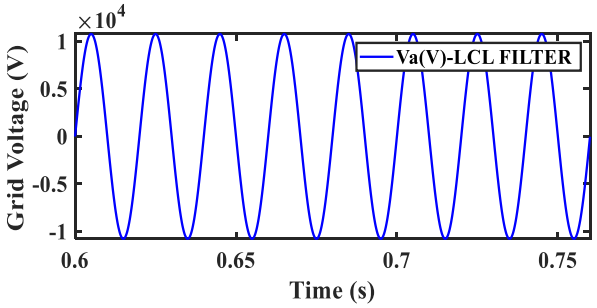

FIGURE 24. Output current signal with LCL-filter design.

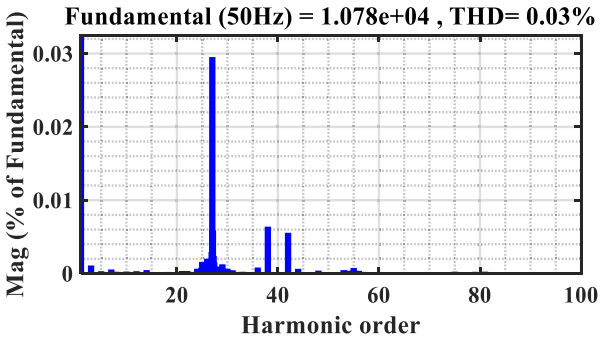

FIGURE 25. Harmonic spectra for output voltage signal with LCL filter design.

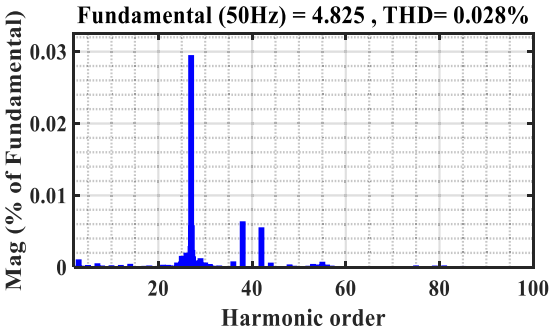

FIGURE 26. Harmonic spectra for output current signal with LCL filter design.

TABLE 7. THD Comparison of the suggested Filters design.

Filters	I-THD	V-THD
Without	13.92	12.73
With LC	8.21	11.3
With LCL	0.03	0.028

TABLE 8. Comparing the traditional design approach with the evolutionary search techniques (GA and GRG) for the LCL filter.

Filter parameter	Conventional design	Evolutionary search approach	
		GA	GRG (proposed)
Cmax (F)	5.969835e-08	5.0532e-08	3.9789e-08
L1 (H)	0.03315	0.0220	0.0221
L2 (H)	0.06495	0.01689	0.0133
R_d (Ω)	228.178	193.19	152.12

that's according to the voltage HD limits of the PV systems standard is rejected.

Figures 23 and 24 show the outputs of the system with an LCL filter. The THD of each voltage and current with an LCL filter is shown in Fig. 25 and Fig. 26, respectively. From Figs. 25 and 26, we find that when using the LCL filter, the THD of current decreased using the LCL filter in the waveform from 13.92 to 0.028 this is according to the current HD limits of the PV systems standard enhancement. We also find that the THD of voltage decreased using the LCL filter in the waveform from 12.73 to 0.03 this is according to the voltage HD limits of the PV systems standard is an improvement.

Due to the addition of the LCL filter, the HD was mostly attenuated. These steps were repeated with different design filters and the THD is calculated for each design for comparison purposes. Table 7 shows the THD of all filters designed without and with filters and Table 8 Comparison between the conventional design method, the GA approach, and the proposed GRG technique for the LCL filter.

THD is a metric for waveform purity and is frequently used to assess how well the filter functions. An LCL filter often has a lesser THD than an LC. This is due to the fact that an LCL

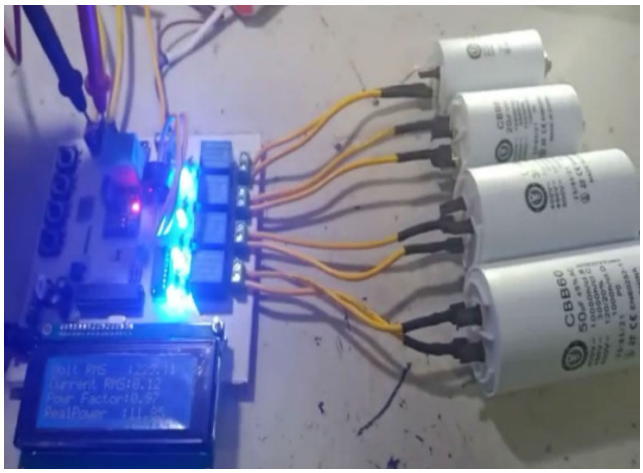

FIGURE 27. Implemented LCL filter.

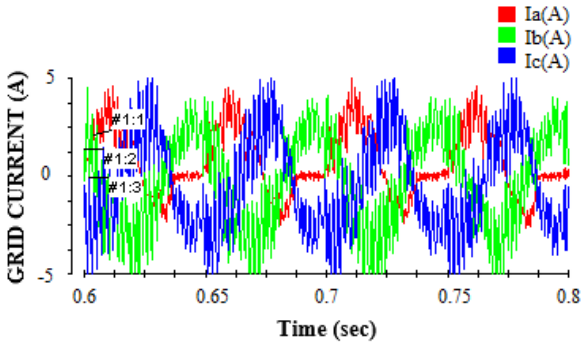

FIGURE 28. Current waveform before filtering by LCL filter.

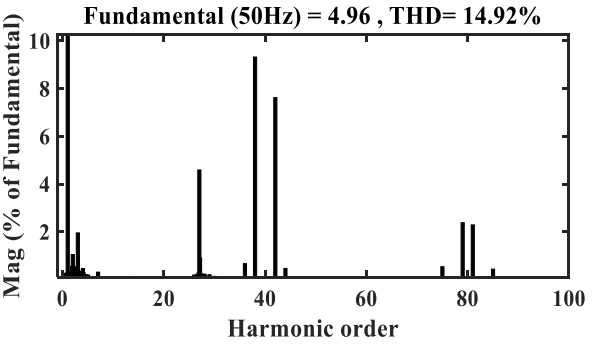

FIGURE 29. Total and individual harmonics levels of the output current waveform before filtering by LCL filter.

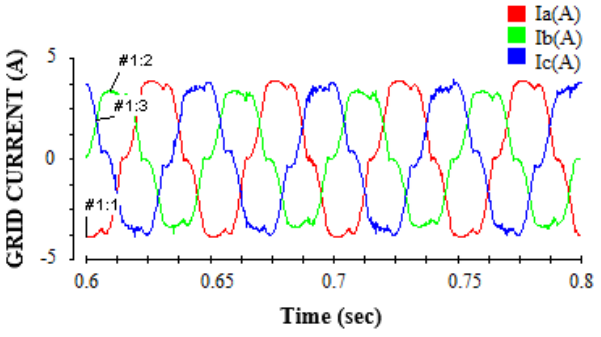

FIGURE 30. Current waveform after filtering by LCL filter.

reduces the level of harmonics of the waveform supplied by connecting a series L and a parallel C to the load. A larger THD may result from an LC filter's single series L or parallel C. Furthermore, compared to LC types, LCL types are more effective at suppressing high-order HD. This is due to the fact that an LCL type has a large damping capacity for upper-order harmonics that a load may produce. It's important to keep in mind that the precise comparison of THD between LC and LCL sorts will rely on the particular design and operating circumstances. LCL kinds are typically more appropriate than LC filters for tasks that call for minimal THD, such as PQ enhancement.

Most LCL design approaches include hand-tuning of design factors like element values and structure. This can be a labor-intensive and iterative process, and the designer must draw on their knowledge and experience to produce a successful design. On the other hand, evolutionary search methods, including GA and GRG, utilize an optimization algorithm that resembles the procedure of nature choice to identify the best design. These approaches are analytically costly but may swiftly examine the architectural space and identify solutions that are close to ideal, frequently requiring fewer manual tweaks. In terms of computing efficiency, GRG is superior to GA, but if the design space is complicated, it might not be able to locate the global optimum.

A. EXPERIMENTAL RESULTS OF DESIGN FILTER

The proposed LCL has been validated using a grid-connected three-phase 115 W inverter prototype with the ability to operate in a stand-alone mode. The LCL filter is shown in Fig. 27, based on parameter values listed in Table 8, has been designed and built. The control algorithm was executed in a dSPACE 1104 real-time platform. Even though the system had been constructed utilizing appropriate control techniques and tools, as illustrated in Figs. 28 and 29, the I-THD had been greater than the usual threshold for distortion elimination. It may be noticed that the present waveform's harmonics oscillated at a frequency of 14. 92 percent. As a result, the efficacy of the suggested system was enhanced, and the I-THD has been lowered to 3% as demonstrated in Figs. 30 and 31. This was accomplished by designing the LCL filter efficiently and increasing the switching frequency. Figs. 28 and 30 show the current signal preceding and following the LCL filter, respectively. Evidently, the overall harmonic oscillations in the application filter design in a PV system are now decreased from 14.92% to 3% after filtering because of an LCL filter. Furthermore, the designed filter values is Cmax $_{(F)=}$50 UF, L1 $_{(H)}$ = 30 mH, L2 $_{(H)=}$54 mH, and $R_{d(\Omega)=}$1.6 k.

The V-THD had been greater than the usual threshold for distortion elimination. It may be noticed that the

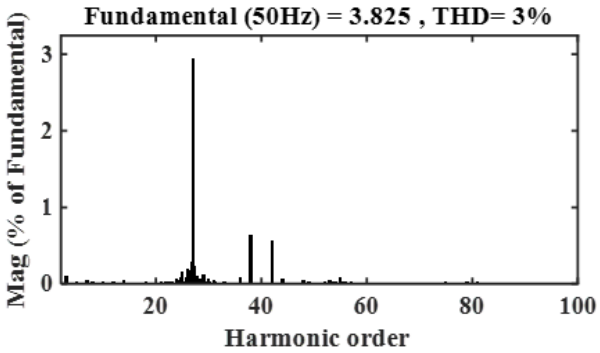

FIGURE 31. Total and individual harmonics levels of the output current waveform after filtering by LCL filter.

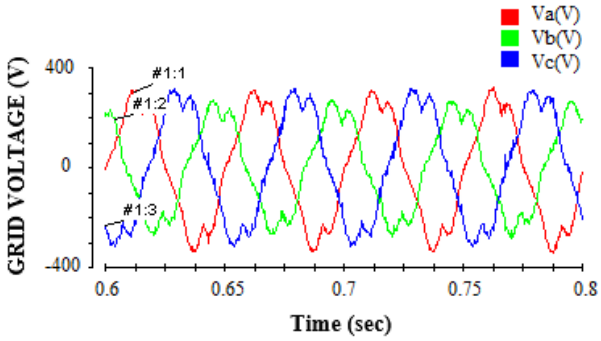

FIGURE 32. Voltage waveform before filtering by LCL filter.

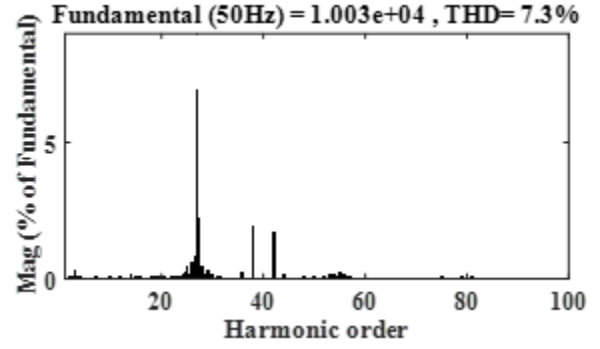

FIGURE 33. Total and individual harmonics levels of the output voltage waveform before filtering by LCL filter.

present waveform's harmonics oscillated at a frequency of 7.3 percent. As a result, the efficacy of the suggested system was enhanced, and the VTHD has been lowered to 0.029% as demonstrated in Figs. 33 and 35. This was accomplished by designing the LCL filter efficiently and increasing the switching frequency. Figures 32 and 34 show the voltage signal preceding and following the LCL filter, respectively. Evidently, the overall harmonic oscillations in the application filter design in a PV system are now decreased from 7.3% to 0.029% after filtering because of an LCL filter.

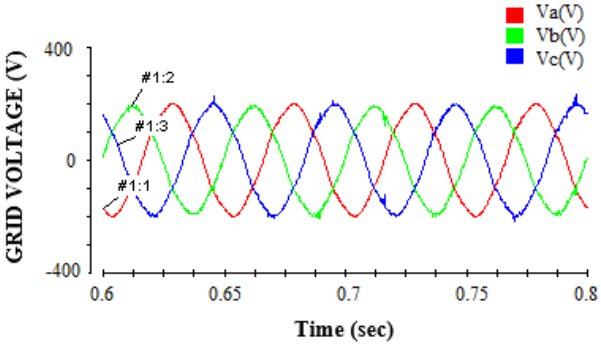

FIGURE 34. Voltage waveform after filtering by LCL filter.

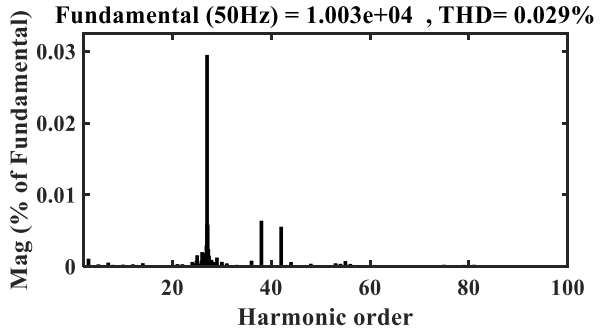

FIGURE 35. Total and individual harmonics levels of the output voltage waveform after filtering by LCL filter.

VII. CONCLUSION

In this study, MPPT based on two alternative methods (ANN and CS) for a GCPV system is investigated. The additional benefit of ANN is that it tracks environmental conditions more quickly than CS systems. Due to its changeable step size, the ANN approach produces a steady response for computing MPP. It also improved the profile of PV power, voltage, current, and D using a number of control methods. All of the schemes had extremely high THD at first, but once the designed and proposed filter has been added, THD dropped to less than 1%, which is within acceptable limits. Passive damping techniques are employed and described in this work. The Matlab/Simulink toolbox (LC, and LCL) is used to assess several typologies for a 100 kW three-phase inverter GCPV system. The damped LCL filter with a series resistor is the best option, as demonstrated by the reduction of the total harmonic destruction current from 14.92 to 3%, and reduction of the THD voltage from 7.3 to 0.029%, and the suppression of the resonant peak.

CONFLICT OF INTEREST

The authors declare that they have no conflict of interest concerning the publication of this article.

DATA AVAILABILITY STATEMENT

Data sharing is not applicable to this article as no datasets were generated or analyzed during the current study.

REFERENCES

[1] M. Woźniak, A. Badora, K. Kud, and L. Woźniak, "Renewable energy sources as the future of the energy sector and climate in Poland—Truth or myth in the opinion of the society," *Energies*, vol. 15, no. 1, p. 45, Dec. 2021, doi: 10.3390/en15010045.

[2] M. Fadaeenejad, M. A. M. Radzi, M. Fadaeenejad, M. Zarif, and Z. Gandomi, "Optimization and comparison analysis for application of PV panels in three villages," *Energy Sci. Eng.*, vol. 3, no. 2, pp. 145–152, Mar. 2015, doi: 10.1002/ese3.52.

[3] H. K. Jahan, M. Abapour, K. Zare, S. H. Hosseini, F. Blaabjerg, and Y. Yang, "A multilevel inverter with minimized components featuring self-balancing and boosting capabilities for PV applications," *IEEE J. Emerg. Sel. Topics Power Electron.*, vol. 11, no. 1, pp. 1169–1178, Feb. 2023, doi: 10.1109/JESTPE.2019.2922415.

[4] V. V. Tyagi, N. A. A. Rahim, N. A. Rahim, and J. A. L. Selvaraj, "Progress in solar PV technology: Research and achievement," *Renew. Sustain. Energy Rev.*, vol. 20, pp. 443–461, Apr. 2013, doi: 10.1016/j.rser.2012.09.028.

[5] K. Kumari and A. K. Jain, "Sensor reduction of a PV-grid tied system with tripartite control based on LCL filter," *IET Energy Syst. Integr.*, vol. 4, no. 3, pp. 409–419, Sep. 2022, doi: 10.1049/esi2.12072.

[6] M. M. Mahmoud, H. S. Salama, M. Bajaj, M. M. Aly, I. Vokony, S. S. H. Bukhari, D. E. M. Wapet, and A.-M.-M. Abdel-Rahim, "Integration of wind systems with SVC and STATCOM during various events to achieve FRT capability and voltage stability: Towards the reliability of modern power systems," *Int. J. Energy Res.*, vol. 2023, pp. 1–28, Feb. 2023, doi: 10.1155/2023/8738460.

[7] N. K. Saxena, A. R. Gupta, S. Mekhilef, W. D. Gao, A. Kumar, V. Gupta, R. S. Netto, and A. Kanungo, "Firefly algorithm based LCL filtered grid-tied STATCOM design for reactive power compensation in SCIG based micro-grid," *Energy Rep.*, vol. 8, pp. 723–740, Nov. 2022, doi: 10.1016/j.egyr.2022.07.106.

[8] H. Boudjemai, S. A. E. M. Ardjoun, H. Chafouk, M. Denai, Z. M. S. Elbarbary, A. I. Omar, and M. M. Mahmoud, "Application of a novel synergetic control for optimal power extraction of a small-scale wind generation system with variable loads and wind speeds," *Symmetry*, vol. 15, no. 2, p. 369, Jan. 2023, doi: 10.3390/sym15020369.

[9] V. R. Chowdhury and A. Singh, "Adaptive internal model based current control with embedded active damping of a three-phase grid-connected inverter with LCL filter for PV application," in *Proc. IEEE Energy Convers. Congr. Expo. (ECCE)*, Oct. 2022, pp. 1–6, doi: 10.1109/ECCE50734.2022.9947896.

[10] S. Foteinis, N. Savvakis, and T. Tsoutsos, "Energy and environmental performance of photovoltaic cooling using phase change materials under the Mediterranean climate," *Energy*, vol. 265, Feb. 2023, Art. no. 126355, doi: 10.1016/j.energy.2022.126355.

[11] G. Walker, "Evaluating MPPT converter topologies using a MATLAB PV model," *J. Electr. Electron. Eng. Aust.*, vol. 21, no. 1, pp. 49–55, 2001.

[12] A. Mohapatra, B. Nayak, P. Das, and K. B. Mohanty, "A review on MPPT techniques of PV system under partial shading condition," *Renew. Sustain. Energy Rev.*, vol. 80, pp. 854–867, Dec. 2017, doi: 10.1016/j.rser.2017.05.083.

[13] I. Villanueva, N. Vázquez, J. Vaquero, C. Hernández, H. López, and R. Osorio, "L vs. LCL filter for photovoltaic grid-connected inverter: A reliability study," *Int. J. Photoenergy*, vol. 2020, pp. 1–10, Jan. 2020, doi: 10.1155/2020/7872916.

[14] A. S. Chatterjee, "A bus clamping PWM-based improved control of grid tied PV inverter with LCL filter under varying grid frequency condition," *IETE J. Res.*, vol. 69, no. 2, pp. 862–878, Feb. 2023, doi: 10.1080/03772063.2020.1844067.

[15] V. R. Vakacharla, K. Gnana, P. Xuewei, B. L. Narasimaharaju, M. Bhukya, A. Banerjee, R. Sharma, and A. K. Rathore, "State-of-the-art power electronics systems for solar-to-grid integration," *Sol. Energy*, vol. 210, pp. 128–148, Nov. 2020, doi: 10.1016/j.solener.2020.06.105.

[16] A. R. Jordehi, "Maximum power point tracking in photovoltaic (PV) systems: A review of different approaches," *Renew. Sustain. Energy Rev.*, vol. 65, pp. 1127–1138, Nov. 2016, doi: 10.1016/j.rser.2016.07.053.

[17] B. Yang, T. Zhu, J. Wang, H. Shu, T. Yu, X. Zhang, W. Yao, and L. Sun, "Comprehensive overview of maximum power point tracking algorithms of PV systems under partial shading condition," *J. Cleaner Prod.*, vol. 268, Sep. 2020, Art. no. 121983, doi: 10.1016/j.jclepro.2020.121983.

[18] M. Hosseinpour and N. Rasekh, "A single-phase grid-tied PV based Trans-Z-source inverter utilizing LCL filter and grid side current active damping," *J. Energy Manag. Technol.*, vol. 3, no. 3, pp. 67–77, 2019.

[19] E. Rakhshani, K. Rouzbehi, A. J. Sánchez, A. C. Tobar, and E. Pouresmaeil, "Integration of large scale PV-based generation into power systems: A survey," *Energies*, vol. 12, no. 8, p. 1425, Apr. 2019, doi: 10.3390/en12081425.

[20] D. P. Mishra, K. K. Rout, S. Mishra, M. Nivas, R. K. P. R. Naidu, and S. R. Salkuti, "Power quality enhancement of grid-connected PV system," *Int. J. Power Electron. Drive Syst.*, vol. 14, no. 1, pp. 369–377, 2023, doi: 10.11591/ijpeds.v14.i1.pp369-377.

[21] M. M. Rana, M. Uddin, M. R. Sarkar, G. M. Shafiullah, H. Mo, and M. Atef, "A review on hybrid photovoltaic—Battery energy storage system: Current status, challenges, and future directions," *J. Energy Storage*, vol. 51, Jul. 2022, Art. no. 104597, doi: 10.1016/j.est.2022.104597.

[22] H. H. Figueira, H. L. Hey, L. Schuch, C. Rech, and L. Michels, "Brazilian grid-connected photovoltaic inverters standards: A comparison with IEC and IEEE," in *Proc. IEEE 24th Int. Symp. Ind. Electron. (ISIE)*, Jun. 2015, pp. 1104–1109, doi: 10.1109/ISIE.2015.7281626.

[23] P. S. de Oliveira, M. A. A. Lima, A. S. Cerqueira, C. A. Duque, and D. D. Ferreira, "Harmonic analysis based on scica at PCC of a grid-connected micro solar PV power plant," in *Proc. 18th Int. Conf. Harmon. Quality Power (ICHQP)*, May 2018, pp. 1–6, doi: 10.1109/ICHQP.2018.8378875.

[24] A. Vinayagam, A. Aziz, P. M. Balasubramaniyam, J. Chandran, V. Veerasamy, and A. Gargoom, "Harmonics assessment and mitigation in a photovoltaic integrated network," *Sustain. Energy, Grids Netw.*, vol. 20, Dec. 2019, Art. no. 100264, doi: 10.1016/j.segan.2019.100264.

[25] S. K. Das, M. K. Sinha, and A. K. Prasad, "Designing and simulation of double stage grid-linked PV system using MATLAB/simulink," in *Recent Advances in Power Systems* (Lecture Notes in Electrical Engineering), vol. 960, 2023, pp. 169–195, doi: 10.1007/978-981-19-6605-7_13.

[26] R. Chen, J. Zeng, X. Huang, and J. Liu, "An H_∞ filter based active damping control strategy for grid-connected inverters with LCL filter applied to wind power system," *Int. J. Electr. Power Energy Syst.*, vol. 144, Jan. 2023, Art. no. 108590, doi: 10.1016/j.ijepes.2022.108590.

[27] B. Singh, A. Verma, and V. K. Giri, "Design of LCL filter in front–end inverters for grid interfaced electric generation," in *Proc. 6th Int. Conf. Advance Comput. Intell. Eng.*, in Lecture Notes in Networks and Systems, vol. 428, 2023, pp. 681–689, doi: 10.1007/978-981-19-2225-1_59.

[28] B. Supriya, K. Palle, A. Bhanuchandar, R. Sakile, D. Vamshy, and K. B. Kumar, "A current control scheme of three phase three-level neutral point clamped grid connected inverter using min–max algorithm approach," in *Smart Energy and Advancement in Power Technologies* (Lecture Notes in Electrical Engineering), vol. 927, 2023, pp. 257–266, doi: 10.1007/978-981-19-4975-3_20.

[29] A. Tripathi, S. P. Soundharya, R. Vigneshwar, and M. R. Rashmi, "Concatenation of SEPIC and matrix converter with LCL filter for vehicle to grid application," in *Pervasive Computing and Social Networking* (Lecture Notes in Networks and Systems), vol. 475, 2023, pp. 743–757, doi: 10.1007/978-981-19-2840-6_56.

[30] M. H. Arshad, S. El-Farik, M. Abido, Mati-Ur-Rasool, and M. I. Hossain, "Genetic algorithm tuned adaptive discrete-time sliding mode controller for grid-connected inverter with an LCL filter," *Energy Rep.*, vol. 8, pp. 623–640, Nov. 2022, doi: 10.1016/j.egyr.2022.09.179.

[31] D. Datta, S. K. Sarker, and M. R. I. Sheikh, "Designing a unified damping and cross-coupling rejection controller for LCL filtered PV-based islanded microgrids," *Eng. Sci. Technol., Int. J.*, vol. 35, Nov. 2022, Art. no. 101244, doi: 10.1016/j.jestch.2022.101244.

[32] R. Xu, L. Xia, J. Zhang, and J. Ding, "Design and research on the LCL filter in three-phase PV grid-connected inverters," *Int. J. Comput. Electr. Eng.*, vol. 5, no. 3, pp. 322–325, 2013, doi: 10.7763/ijcee.2013.v5.723.

[33] S. Adak, H. Cangi, and A. S. Yilmaz, "Design of an LLCL type filter for stand-alone PV systems' harmonics," *J. Energy Syst.*, vol. 3, no. 1, pp. 36–50, Mar. 2019, doi: 10.30521/jes.506076.

[34] Y. Lei, W. Xu, C. Mu, Z. Zhao, H. Li, and Z. Li, "New hybrid damping strategy for grid-connected photovoltaic inverter with LCL filter," *IEEE Trans. Appl. Supercond.*, vol. 24, no. 5, pp. 1–8, Oct. 2014, doi: 10.1109/TASC.2014.2351237.

[35] H. Yu, J. Pan, and A. Xiang, "A multi-function grid-connected PV system with reactive power compensation for the grid," *Sol. Energy*, vol. 79, no. 1, pp. 101–106, Jul. 2005, doi: 10.1016/j.solener.2004.09.023.

[36] M. Andela, A. Shaik, S. Beemagoni, V. Kurimilla, R. Veramalla, A. Kodakkal, and S. R. Salkuti, "Solar photovoltaic system-based reduced switch multilevel inverter for improved power quality," *Clean Technol.*, vol. 4, no. 1, pp. 1–13, Jan. 2022, doi: 10.3390/cleantechnol4010001.

[37] A. Fekik, M. L. Hamida, H. Houassine, A. T. Azar, N. A. Kamal, H. Denoun, S. Vaidyanathan, and A. Sambas, "Power quality improvement for grid-connected photovoltaic panels using direct power control," in *Modeling and Control of Static Converters for Hybrid Storage Systems*, 2021, pp. 107–142, doi: 10.4018/978-1-7998-7447-8.ch005.

[38] D. Prasad, N. Kumar, and R. Sharma, "Shunt active power filter based on synchronous reference frame theory connected to SPV for power quality enrichment," in *Machine Learning, Advances in Computing, Renewable Energy and Communication* (Lecture Notes in Electrical Engineering), vol. 768, 2022, pp. 281–292, doi: 10.1007/978-981-16-2354-7_26.

[39] W. A. A. Salem, W. G. Ibrahim, A. M. Abdelsadek, and A. A. Nafeh, "Grid connected photovoltaic system impression on power quality of low voltage distribution system," *Cogent Eng.*, vol. 9, no. 1, Dec. 2022, Art. no. 2044576, doi: 10.1080/23311916.2022.2044576.

[40] M. Awad, M. M. Mahmoud, Z. M. S. Elbarbary, L. M. Ali, S. N. Fahmy, and A. I. Omar, "Design and analysis of photovoltaic/wind operations at MPPT for hydrogen production using a PEM electrolyzer: Towards innovations in green technology," *PLoS ONE*, vol. 18, no. 7, Jul. 2023, Art. no. e0287772, doi: 10.1371/journal.pone.0287772.

[41] M. Awad, A. M. Ibrahim, Z. M. Alaas, A. El-Shahat, and A. I. Omar, "Design and analysis of an efficient photovoltaic energy-powered electric vehicle charging station using perturb and observe MPPT algorithm," *Frontiers Energy Res.*, vol. 10, pp. 1–22, Aug. 2022, doi: 10.3389/fenrg.2022.969482.

[42] M. H. Mahlooji, H. R. Mohammadi, and M. Rahimi, "A review on modeling and control of grid-connected photovoltaic inverters with LCL filter," *Renew. Sustain. Energy Rev.*, vol. 81, pp. 563–578, Jan. 2018, doi: 10.1016/j.rser.2017.08.002.

[43] F. Gao, R. Hu, and L. Yin, "Variable boundary reinforcement learning for maximum power point tracking of photovoltaic grid-connected systems," *Energy*, vol. 264, Feb. 2023, Art. no. 126278, doi: 10.1016/j.energy.2022.126278.

[44] R. Santhi and A. Srinivasan, "An efficient AOA-RERNN control approach for a non-isolated quasi-Z-source novel multilevel inverter based grid connected PV system," *Energy*, vol. 263, Jan. 2023, Art. no. 125492, doi: 10.1016/j.energy.2022.125492.

[45] A. Atoui, M. Kermadi, M. S. Boucherit, K. Benmansour, S. Barkat, F. Akel, and S. Mekhilef, "A fast and accurate global maximum power point tracking controller for photovoltaic systems under complex partial shadings," *Int. J. Electr. Comput. Eng.*, vol. 13, no. 1, pp. 69–84, 2023, doi: 10.11591/ijece.v13i1.pp69-84.

[46] A. Ghatak, T. Pandit, D. Kishan, and R. Raushan, "Comparative analysis of maximum power point tracking algorithms for standalone PV system under variable weather conditions," *Distrib. Gener. Alternative Energy J.*, vol. 38, no. 1, pp. 215–248, 2022, doi: 10.13052/dgaej2156-3306.38110.

[47] A. M. Jasim, B. H. Jasim, S. Mohseni, and A. C. Brent, "Consensus-based dispatch optimization of a microgrid considering meta-heuristic-based demand response scheduling and network packet loss characterization," *Energy AI*, vol. 11, Jan. 2023, Art. no. 100212, doi: 10.1016/j.egyai.2022.100212.

[48] S. K. R. Moosavi, M. Mansoor, M. H. Zafar, N. M. Khan, A. F. Mirza, and N. Akhtar, "Highly efficient maximum power point tracking control technique for PV system under dynamic operating conditions," *Energy Rep.*, vol. 8, pp. 13529–13543, Nov. 2022, doi: 10.1016/j.egyr.2022.10.011.

[49] M. Inci and A. Caliskan, "Performance enhancement of energy extraction capability for fuel cell implementations with improved cuckoo search algorithm," *Int. J. Hydrogen Energy*, vol. 45, no. 19, pp. 11309–11320, Apr. 2020, doi: 10.1016/j.ijhydene.2020.02.069.

[50] M. M. Mahmoud, B. S. Atia, Y. M. Esmail, S. A. E. M. Ardjoun, N. Anwer, A. I. Omar, F. Alsaif, S. Alsulamy, and S. A. Mohamed, "Application of whale optimization algorithm based FOPI controllers for STATCOM and UPQC to mitigate harmonics and voltage instability in modern distribution power grids," *Axioms*, vol. 12, no. 5, p. 420, Apr. 2023, doi: 10.3390/axioms12050420.

[51] J. Faria, J. Pombo, M. Do Rosário Calado, and S. Mariano, "Current control optimization for grid-tied inverters using cuckoo search algorithm," *KnE Eng.*, Jun. 2020, doi: 10.18502/keg.v5i6.7099.

[52] F. K. Abo-Elyousr, A. M. Abdelshafy, and A. Y. Abdelaziz, "MPPT-based particle swarm and cuckoo search algorithms for PV systems," in *Modern Maximum Power Point Tracking Techniques for Photovoltaic Energy Systems* (Green Energy and Technology), 2020, pp. 379–400, doi: 10.1007/978-3-030-05578-3_14.

[53] M. Z. Rosselan and S. I. Sulaiman, "Dolphin echolocation algorithm for optimal sizing of grid-connected photovoltaic system," in *Proc. IEEE Int. Conf. Appl. Syst. Invention (ICASI)*, Apr. 2018, pp. 1252–1255, doi: 10.1109/ICASI.2018.8394518.

[54] S. Banerjee, "Advanced task scheduling for cloud service provider using genetaic algorithm," *IOSR J. Eng.*, vol. 2, no. 7, pp. 141–147, Jul. 2012, doi: 10.9790/3021-0271141147.

[55] A. A. Emam, H. E. Keshta, M. A. Mosa, and A. A. Ali, "Bi-level energy management system for optimal real time operation of grid tied multi-nanogrids," *Electr. Power Syst. Res.*, vol. 214, Jan. 2023, Art. no. 108957, doi: 10.1016/j.epsr.2022.108957.

[56] T. D. C. Busarello, K. Zeb, and M. G. Simões, "Highly accurate digital current controllers for single-phase LCL-filtered grid-connected inverters," *Electricity*, vol. 1, no. 1, pp. 12–36, Jul. 2020, doi: 10.3390/electricity1010002.

[57] R. D. A. Raj, T. Aditya, and M. R. Shinde, "Power quality enhancement of grid-connected solar photovoltaic system using LCL filter," in *Proc. Int. Conf. Power Electron. IoT Appl. Renew. Energy Control (PARC)*, Feb. 2020, pp. 334–339, doi: 10.1109/PARC49193.2020.236621.

[58] F. Mulolani, A. Althobaiti, and Y. Alamoudi, "Notch-filter active damping of LCL filter resonance in a grid-connected inverter with variable grid inductance," in *Proc. Adv. Sci. Eng. Technol. Int. Conf. (ASET)*, Mar. 2019, doi: 10.1109/ICASET.2019.8714393.

NAGWA F. IBRAHIM received the B.Sc., M.Sc., and Ph.D. degrees from the Faculty of Industrial Education, Suez Canal University, Suez, Egypt, in 2008, 2015, and 2019, respectively. She is currently an Assistant Professor with the Department of Electrical Power and Machine, Faculty of Technology and Education, Suez University. Her research interests include renewable energy sources, power system protection, power electronics, high voltage direct current (HVDC), control and power quality issues, and the control of power electronic converters and electrical machine drives.

MOHAMED METWALLY MAHMOUD was born in Sohag, Egypt. He received the B.Sc., M.Sc., and Ph.D. degrees in electrical engineering from Aswan University, Egypt, in 2015, 2019, and 2020, respectively. He is currently a Professor (Assistant) with Aswan University, the Director of the Quality Assurance Unit, and an Executive Director of the Continuous Improvement and Qualification for Accreditation Program. His research interests include the performance improvement of wind generators, optimization methods, intelligent controllers, fault ride through capability, power quality, FACTS tools, and energy storage systems. He has been awarded Aswan University prizes for international publishing, in 2020, 2021, and 2022, respectively.

ALI M. H. AL THAIBAN was born in Saudi Arabia, in 1988. He received the B.Sc. and M.Sc. degrees in electrical engineering from Fahd Bin Sultan University, Saudi Arabia, in 2013 and 2020, respectively. He is currently pursuing the Ph.D. degree in electrical engineering with Mansoura University, Mansoura, Egypt. He is also an Employee of Health Ministry at the Safety and Maintenance, Saudi Arabia.

ABDULWASA B. BARNAWI was born in Saudi Arabia, Makkah, in April 1981. He received the B.Sc. degree in electrical power engineering from the Yanbu Industrial College, Yanbu, Saudi Arabia, in 2007, the M.Sc. degree in electrical engineering from the University of New Haven, USA, West Haven, CT, USA, in 2012, and the Ph.D. degree in electrical engineering from the Department of Electrical Engineering and Computer Science, The University of Toledo, USA, Toledo, OH, USA, in 2016. Since 2019, he has been with the Department of Electrical Engineering, King Khalid University, Saudi Arabia, Abha, as an Assistant Professor. His current research interests include renewable energy integration, power system planning, generation adequacy evaluation, energy management (applying priced based demand response strategies), smart grid, and dynamic electricity pricing.

Z. M. S. ELBARBARY was born in Kafrelsheikh, Egypt, in April 1971. He received the B.Sc., M.Sc., and Ph.D. degrees in electrical engineering from Menoufia University, Shebin El-Kom, Egypt, in 1994, 2002, and 2007, respectively. In 2009, he joined Kafrelsheikh University as an Assistant Professor. He was a Research Visitor with Ghent University, Ghent, Belgium, in 2016. He promoted to a Full Professor in power electronics, in June 2022. His research interests include the control of electrical machines, senseless control, the applications of power electronics, real-time control using digital signals processing, and renewable energy applications.

AHMED IBRAHIM OMAR was born in Cairo, Egypt, in September 1989. He received the B.Sc. degree (Hons.) in electrical power and machines engineering from The Higher Institute of Engineering at El-Shorouk, in 2011, and the M.Sc. and Ph.D. degrees in electrical power and machines from the Faculty of Engineering, Cairo University, Egypt, in 2014 and 2019, respectively. He is currently an Assistant Professor with The Higher Institute of Engineering at El-Shorouk City, El-Shorouk Academy, Egypt. His research interests include renewable energy, FACTS in power systems, power quality, smart grid, energy efficiency, optimization and machine learning, green energy, and economics. He is the author or coauthor of many refereed journals and conference papers. He is a Reviewer for several journals, such as *Ain Shams Engineering Journal* and *Journal of Cleaner Production*.

HANY ABDELFATTAH was born in El-Mahalla El-Kubra, Egypt, in 1976. He received the B.Sc. degree (Hons.) in electronic engineering and the M.Sc. degree in control engineering from Mansoura University, Egypt, in 1999 and 2006, respectively, and the Ph.D. degree in electrical power and machine engineering (control specialization) from Cairo University, Egypt, in 2013. He is currently a Professor in control with the Electrical Power Department, Faculty of Technology and Education, Suez University, Egypt. His research interests include power system stability and control, and the robust control of nuclear power plant. He has published 11 papers in automatic control.